ASTRONOMY
AND
ASTROPHYSICS

Neutrino-pair bremsstrahlung by electrons in neutron star crusts

A.D. Kaminker[1], **C.J. Pethick**[2,3], **A.Y. Potekhin**[1], **V. Thorsson**[2,4,⋆], **and D.G. Yakovlev**[1]

[1] Ioffe Physical-Technical Institute, Politekhnicheskaya 26, 194021 St.-Petersburg, Russia
[2] Nordita, Blegdamsvej 17, DK-2100 Copenhagen Ø, Denmark
[3] Department of Physics, University of Illinois at Urbana-Champaign, 1110 West Green Street, Urbana, Illinois 61801-3080, USA
[4] Department of Physics, University of Washington, Box 351560, Seattle, Washington 98195-1560, USA

Abstract. Neutrino-pair bremsstrahlung by relativistic degenerate electrons in a neutron-star crust at densities 10^9 g cm$^{-3} \lesssim \rho \lesssim 1.5 \times 10^{14}$ g cm^{-3} is analyzed. The processes taken into account are neutrino emission due to Coulomb scattering of electrons by atomic nuclei in a Coulomb liquid, and electron-phonon scattering (the phonon contribution) and Bragg diffraction (the static-lattice contribution) in a Coulomb crystal. The static-lattice contribution is calculated including the electron band-structure effects for cubic Coulomb crystals of different types and also for the liquid crystal phases composed of rod- and plate-like nuclei near the bottom of the neutron-star crust (10^{14} g cm$^{-3} \lesssim \rho \lesssim 1.5 \times 10^{14}$ g cm^{-3}). The phonon contribution is evaluated with proper treatment of the multi-phonon processes which removes a jump in the neutrino bremsstrahlung emissivity at the melting point obtained in previous works. Generally, bremsstrahlung in the solid phase does not differ significantly from that in the liquid. At $\rho \lesssim 10^{13}$ g cm^{-3}, the results are rather insensitive to the nuclear form factor, but results for the solid state near the melting point are affected significantly by the Debye–Waller factor and multi-phonon processes. At higher densities the Debye–Waller factor and multi-phonon processes become less important but the nuclear form factor becomes more significant. With growing ρ, the phonon contribution becomes smaller. Near the bottom of the neutron star crust bremsstrahlung becomes less efficient due to the reduction of the effective electron–nucleus matrix element by the electron band-structure effects and the nuclear form factor. A comparison of the various neutrino generation mechanisms in neutron star crusts shows that electron bremsstrahlung is among the most important ones.

Key words: dense matter – stars: neutron

1. Introduction

Neutrino-pair bremsstrahlung of electrons in liquid and crystalline phases of dense matter is one of the major neu-

trino energy-loss mechanisms in neutron star crusts. Here, by bremsstrahlung we mean neutrino emission due to electromagnetic interaction of electrons with atomic nuclei. The process can be written schematically as

$$e + (Z, A) \rightarrow e + (Z, A) + \nu + \bar{\nu}. \tag{1}$$

It proceeds via neutral and charged electroweak currents and leads to emission of neutrinos of all flavors.

For practical application to the thermal evolution of neutron stars, one needs to know the neutrino energy emission rate (emissivity) Q in the density range from about 10^9 g cm^{-3} to 1.5×10^{14} g cm^{-3} (the core-crust interface) at temperatures $T \lesssim 5 \times 10^9$ K (at which the nuclei are not dissociated). Under these conditions, the electrons are strongly degenerate and ultra-relativistic, and the nuclei form either a Coulomb liquid, or a Coulomb crystal. For densities higher than 10^{12}- 10^{13} g cm^{-3}, the melting temperature of the crystal exceeds 5×10^9 K, and the case of a Coulomb liquid is of no practical importance. In the density range from about 10^{14} g cm^{-3} to 1.5×10^{14} g cm^{-3}, the nuclei resemble rods and plates, rather than spheres (Lorenz et al. 1993; Pethick & Ravenhall 1995).

The neutrino-pair bremsstrahlung process (1) in a crystal is formally different from that in a liquid. In the liquid state, neutrinos are generated due to Coulomb scattering of electrons by nuclei. In the solid state, there are two contributions to the process, electron–phonon scattering (electron scattering by the nuclear charge fluctuations due to lattice vibrations, referred to as the *phonon contribution*), and the Bragg diffraction of electrons, which is commonly called the *static-lattice contribution*.

Neutrino-pair bremsstrahlung has been analyzed by a number of authors (see, e.g., Itoh et al. 1989, 1996; Pethick & Thorsson 1997, and references therein). The case of a Coulomb liquid has been thoroughly studied by Festa & Ruderman (1969), Dicus et al. (1976), Soyeur & Brown (1979), Itoh & Kohyama (1983), and, most recently, by Haensel et al. (1996). The phonon contribution in the crystalline lattice has been analyzed by Flowers (1973), Itoh et al. (1984b, 1989), and also by Yakovlev & Kaminker (1996). Notice, however, that all these authors have made use of the so-called one-phonon approximation, whereas, as we shall demonstrate below, multi-phonon scattering processes can give a noticeable contribution especially near the melting point. The static-lattice contribution has been consid-

ered by Flowers (1973) and by Itoh et al. (1984a) neglecting the electron band-structure effects (the presence of gaps in the electron dispersion relation). However, Pethick & Thorsson (1994, 1997) have shown that the band structure can suppress strongly the static-lattice contribution and is thus very important. In particular, Pethick & Thorsson (1997) derived a general expression for the static-lattice contribution.

In the present article, we give an overall analysis of neutrino-pair bremsstrahlung by electrons in neutron star crusts, and obtain formulae convenient for applications. In Sect. 2 we describe briefly physical conditions in neutron star crusts. In Sect. 3 we summarize the formalism for calculating neutrino-pair bremsstrahlung in the liquid and solid phases. While studying the solid phase we consider the ordinary body-centered-cubic (bcc) crystals, as well as face-centered-cubic (fcc) and hexagonal-close-packed (hcp) cubic crystals which can also be formed in neutron-star crusts. The phonon contribution will be calculated using a new approach (Baiko et al. 1998) incorporating multi-phonon effects. It eliminates a jump in the neutrino emissivity at the melting point obtained in previous articles. The static-lattice contribution will be analyzed not only for the traditional phase of spherical nuclei, but also for the 'exotic' phases of nonspherical nuclei. In Sec. 4 we examine the main properties of neutrino-pair bremsstrahlung at various densities and temperatures in neutron-star crusts, and compare bremsstrahlung with other neutrino emission mechanisms. We present also a simple analytic fit for practical evaluation of the neutrino bremsstrahlung energy loss rate.

2. Physical conditions

Let us outline physical conditions in a neutron star envelope at densities $10^9 \, \mathrm{g \, cm^{-3}} \lesssim \rho \lesssim 1.5 \times 10^{14} \, \mathrm{g \, cm^{-3}}$, and at temperatures $T \lesssim 5 \times 10^9$ K (Sect. 1). Matter in these layers consists of electrons and atomic nuclei (ions). At densities higher than the neutron drip density, $\rho_{\mathrm{d}} \approx 4.3 \times 10^{11} \, \mathrm{g \, cm^{-3}}$, free neutrons appear between the nuclei (e.g., Negele & Vautherin 1973). At $\rho \gtrsim 10^{14} \, \mathrm{g \, cm^{-3}}$, the nuclei are likely to form nonspherical clusters (Lorenz et al. 1993; Oyamatsu 1993; Pethick & Ravenhall 1995).

The state of degenerate electrons is characterized by the Fermi momentum $p_{\mathrm{F}} \equiv \hbar k_{\mathrm{F}}$ or the relativistic parameter x:

$$p_{\mathrm{F}} = \hbar (3\pi^2 n_{\mathrm{e}})^{1/3}, \quad x = \frac{p_{\mathrm{F}}}{m_{\mathrm{e}} c} \approx 100.9 \, (\rho_{12} Y_{\mathrm{e}})^{1/3}, \qquad (2)$$

where $Y_{\mathrm{e}} = n_{\mathrm{e}}/n_{\mathrm{b}}$ is the number of electrons per baryon, n_{e} is the number density of electrons, n_{b} the number density of baryons, and ρ_{12} is mass density in units of $10^{12} \, \mathrm{g \, cm^{-3}}$. In the density range under study the electrons are ultra-relativistic ($x \gg 1$). The electron degeneracy temperature is

$$T_{\mathrm{F}} = (\sqrt{1+x^2} - 1) \, T_0, \quad T_0 = \frac{m_{\mathrm{e}} c^2}{k_{\mathrm{B}}} \approx 5.930 \times 10^9 \, \mathrm{K}, \, (3)$$

where k_{B} is the Boltzmann constant. In our case $T \lesssim 5 \times 10^9$ K, and the electrons are strongly degenerate.

The nuclear composition of neutron-star envelopes is not very well known, although it is quite certain that light elements such as H and He transform into heavier ones at densities which are lower than the densities of interest. For simplicity, we assume that only one nuclear species is present at any fixed density (pressure). This leads to discontinuous variations of the nuclear composition with density (pressure). The temperature dependence of the nuclear composition can be ignored at $T < 5 \times 10^9$ K (e.g., Haensel et al. 1996). For illustration, we shall make use of two models of matter in a neutron-star crust: ground-state (cold-catalyzed) matter and accreted matter. For describing ground-state matter, we shall use the following data: the results of Haensel & Pichon (1994) at $\rho < \rho_{\mathrm{d}}$ based on new laboratory measurements of nuclear masses with large neutron excess, the results of Negele & Vautherin (1973) for spherical nuclei at $\rho_{\mathrm{d}} \lesssim \rho \lesssim 1.5 \times 10^{14} \, \mathrm{g \, cm^{-3}}$ derived by a modified Hartree-Fock method, and model I of Oyamatsu (1993), which takes into account nonspherical nuclei. We shall adopt the composition of accreted matter calculated by Haensel & Zdunik (1990) for $\rho \lesssim 10^{13} \, \mathrm{g \, cm^{-3}}$, and we shall not consider accreted matter at higher densities. Accreted matter consists of lighter nuclei, and neutron drip is shifted to higher density as compared to ground-state matter (Fig. 1).

The state of spherical nuclei is determined by the ion-coupling parameter

$$\Gamma = \frac{Z^2 e^2}{a k_{\mathrm{B}} T} \approx 0.225 \, x \, \frac{Z^{5/3}}{T_8}, \qquad (4)$$

where Ze is the nuclear charge, $a = [3/(4\pi n_{\mathrm{i}})]^{1/3}$ is the ion-sphere (Wigner–Seitz cell) radius, $n_{\mathrm{i}} = n_{\mathrm{e}}/Z$ is the number density of nuclei, and T_8 is the temperature in units of 10^8 K. For the densities and temperatures of interest, the spherical nuclei constitute either a strongly-coupled Coulomb liquid ($1 < \Gamma < \Gamma_{\mathrm{m}}$), or a Coulomb crystal ($\Gamma > \Gamma_{\mathrm{m}}$), where Γ_{m}=172 corresponds to solidification of a classical one-component Coulomb liquid into a bcc lattice (Nagara et al. 1987). Thus the melting temperature is

$$T_{\mathrm{m}} = \frac{Z^2 e^2}{a k_{\mathrm{B}} \Gamma_{\mathrm{m}}} \approx 1.32 \times 10^7 Z^{5/3} (\rho_{12} Y_{\mathrm{e}})^{1/3} \, \mathrm{K}. \qquad (5)$$

The density profiles of T_{m} for the ground-state and accreted matter are presented in Fig. 1. The melting temperature of accreted matter is systematically lower due to the lower values of Z. If $\rho > 10^{13} \, \mathrm{g \, cm^{-3}}$, one has $T_{\mathrm{m}} \gtrsim 5 \times 10^9$ K for the ground-state model, and matter is always solid for the conditions under study. A classical bcc lattice is bound most tightly (see, e.g., Brush et al. 1966). Therefore, it is widely assumed that neutron-star crusts are composed of such crystals. However, an fcc or hcp crystal is bound only slightly more weakly, so fcc and hcp crystals may well occur in dense stellar matter along with the bcc ones (e.g., DeWitt et al. 1993; Baiko & Yakovlev 1995), and we shall also consider this possibility.

An important parameter for a Coulomb crystal is the ion plasma temperature

$$T_{\mathrm{p}} = \frac{\hbar \omega_{\mathrm{p}}}{k_{\mathrm{B}}} \approx 7.83 \times 10^9 \left(\frac{Z Y_{\mathrm{e}} \rho_{12}}{A_{\mathrm{i}}} \right)^{1/2} \, \mathrm{K}, \qquad (6)$$
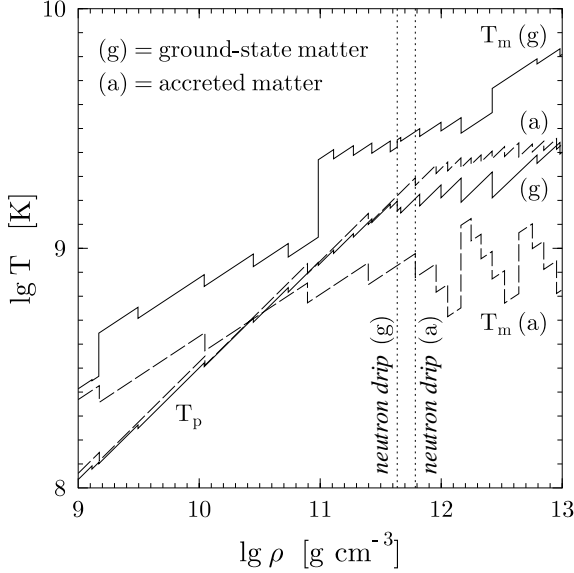
Fig. 1. Density dependence of the melting temperature T_m and the ion plasma temperature T_p, and also neutron drip density (vertical dotted lines) for ground-state matter and accreted matter

which is determined by the ion plasma frequency $\omega_p = \left(4\pi Z^2 e^2 n_i/m_i\right)^{1/2}$, where $m_i \approx A_i m_u$ is the ion mass and $m_u = 1.66 \times 10^{-24}$ g is the atomic mass unit. The plasma temperature characterizes ion vibrations. If $T \gtrsim T_p/8$ the vibrations can be treated classically (the high-temperature case) while at $T \ll T_p$ they should be treated quantum-mechanically (the low-temperature case). In neutron-star crusts, a transition from the high-temperature to the low-temperature regime takes place at temperatures which are lower than T_m (Fig. 1).

We shall consider ion vibrations in a purely Coulomb lattice. For $\rho > \rho_d$ there are neutrons in the space between ions (nuclei). How to include the effect of these neutrons on the lattice dynamics is at present an unsolved problem, and we shall ignore this effect.

The effective interaction between electrons and nuclei depends on a number of effects. One is the character of the Coulomb interaction itself, a second is screening of the interaction by electrons, a third is the shape of the nuclear charge distribution, and a fourth is the effect of thermal vibrations effectively smearing out the nuclear charge, an effect taken into account by inclusion of the Debye–Waller factor. Thus the Fourier transform of the effective electron-ion interaction may be written as

$$V_{\boldsymbol{q}} = \frac{4\pi e \rho_Z \, F(\boldsymbol{q})}{q^2 \, \epsilon(q)} \, e^{-W(q)}, \qquad (7)$$

where ρ_Z is the ion charge per unit volume, $F(\boldsymbol{q})$ is the form factor which reflects the charge distribution within one nucleus, $\epsilon(q)$ is the static longitudinal dielectric factor (Jancovici 1962), and $W(q)$ is the Debye–Waller factor. For a crystal of spherical nuclei, we have $\rho_Z = Z e n_i$; Eq. (7) is valid also for non-

spherical nuclei. The Debye–Waller factor in a crystal of spherical nuclei can be written as

$$W(q) = \frac{\hbar q^2}{4 m_i} \left\langle \frac{\coth(\hbar\omega_s/2k_B T)}{\omega_s} \right\rangle, \qquad (8)$$

where ω_s is a phonon frequency, s enumerates phonon modes and brackets $\langle \ldots \rangle$ denote averaging over phonon wave vectors and polarizations (e.g., Eq. (8) in Yakovlev & Kaminker 1996). In a Coulomb crystal $W = W(q)$ is accurately fitted by Baiko & Yakovlev (1995):

$$W = \frac{\alpha}{2} \left(\frac{q}{2k_F} \right)^2, \quad \alpha = \alpha_0 \left(\frac{1}{2} u_{-1} \, e^{-9.1 t_p} + t_p u_{-2} \right), \ (9)$$

where $t_p = T/T_p$ and

$$\alpha_0 = \frac{4m_e^2 c^2}{k_B T_p m_i} \, x^2 \approx 1.683 \sqrt{\frac{x}{A_i Z}}. \qquad (10)$$

The quantities u_{-1} and u_{-2} are the frequency moments of the phonon spectrum, $u_n = \langle (\omega_s/\omega_p)^n \rangle$. For the bcc lattice, the frequency moments are well known (see, e.g., Pollock & Hansen 1973). For the fcc and hcp crystals, they are easily derived by calculating the phonon spectrum from the Ewald transformation of the lattice sums. The phonon spectra of the bcc, fcc, and hcp lattices appear to be quite similar. Accordingly the properties of these crystals are very similar. In particular, $u_{-1} = 2.798, 2.720$ and 2.703; $u_{-2} = 12.972, 12.143$ and 12.015, for bcc, fcc and hcp lattices, respectively. Note that the frequency moments for the fcc lattice calculated by Baiko & Yakovlev (1995) and used by Baiko & Yakovlev (1996) and Yakovlev & Kaminker (1996) are inaccurate due to erroneous boundaries of the Brillouin zone for this lattice implemented in the momentum averaging scheme. Improved calculations show that Eq. (9) remains valid with the accurate frequency moments for all the lattice types under study. The Debye–Waller factor is important if ion vibrations (either thermal or zero-point ones) are strong.

The simplest nuclear form factor in Eq. (7) corresponds to a spherical atomic nucleus with a uniform proton core of radius R_c:

$$F(q) = \frac{3}{(qR_c)^3} \left[\sin(qR_c) - qR_c \cos(qR_c) \right]. \qquad (11)$$

At $\rho < \rho_d$, the radii of the nuclei do not change under the ambient pressure of neighbouring particles, and one can use the standard formula $R_c = 1.15 \, A^{1/3}$ fm. At these densities the ratio $\eta \equiv R_c/a \ll 1$, and the effect of the atomic form factor is generally negligible ($F(q) \approx 1$ for $q \lesssim 2k_F$). At densities $\rho_d < \rho \lesssim 10^{13}$ g cm^{-3} the simplest form factor remains adequate, but the proton core radius becomes $R_c \approx 1.83 \, Z^{1/3}$ fm as deduced by Itoh & Kohyama (1983) from the results of Negele & Vautherin (1973). In this case, η can be as high as 0.2–0.3 and the effect of the form factor is important. For higher ρ, the proton charge distribution becomes smoother, and the form factor should be modified.

In order to describe accurately all layers of the neutron star crusts we make use of the results by Oyamatsu (1993) who

calculated the local neutron (n) and proton (p) number density distributions within a Wigner–Seitz cell and fitted them in the form

$$
n_j(r) = \begin{cases} (n_j^{\text{in}} - n_j^{\text{out}}) \left[1 - \left(\frac{r}{R_j} \right)^{t_j} \right]^3 + n_j^{\text{out}}, & r < R_j, \\ n_j^{\text{out}}, & r \geq R_j, \end{cases} \quad (12)
$$

where j = n or p, and n_j^{in}, n_j^{out}, t_j and R_j are the fit parameters. These parameters, as well as the sizes of Wigner–Seitz cells, are presented in Table 6 in Oyamatsu (1993) for several selected values of the baryon number density n_{b} for spherical and nonspherical nuclei.

In particular, Oyamatsu (1993) gives the fit parameters for spherical nuclei at three values of baryon number density n_{b}=0.01, 0.03 and 0.055 fm^{-3} (i.e., $\rho = 1.66\times10^{13}, 4.98\times10^{13}$ and 9.13×10^{13} g cm^{-3}) in the inner neutron-star crust. These parameters are quite consistent with those presented by Negele & Vautherin (1973) for nearly the same n_{b}. Some of these parameters can also be deduced from Figs. 3 and 4 and from Table 3 of Negele & Vautherin (1973) for several other values of n_{b} in the inner crust. The parameters appear to be smooth functions of n_{b}, so we interpolated between the given points at $\rho_{\text{d}} \leq \rho \leq 1.4 \times 10^{14}$ g cm^{-3}. This interpolation smears out jumps in the nuclear composition with increasing ρ, but these have little effect on the neutrino-pair bremsstrahlung. The interpolation allows us to calculate easily the parameters of spherical nuclei at any density in the inner crust. In particular, $n_{\text{n}}^{\text{out}}$ gives the number density of free neutrons outside the nuclei ($r > R_{\text{n}}$) while R_{n} may be called the nuclear radius. There are no protons outside nuclei, $n_{\text{p}}^{\text{out}} = 0$, in this regime, and the proton core radius R_{p} is somewhat smaller than R_{n}. The nuclear mass m_{i} is assumed to be that of all nucleons within R_{n}. The parameters t_{n} and t_{p} range from about 4 to 6 and decrease with increasing ρ. Note that the proton core radius R_{p} in Eq. (12) is somewhat larger than the proton core R_{c} in the simplified model (11).

We have obtained also an analytical description of atomic nuclei for lower densities, 10^8 g cm$^{-3} \leq \rho \leq \rho_{\text{d}}$ in the outer neutron-star crust making use of the results by Haensel & Pichon (1994). We have adopted the same parameterization (12) and constructed simple analytic expressions for the nuclear parameters of the ground-state matter as a function of n_{b} in the outer crust. In this case $n_{\text{n}}^{\text{out}} = 0$. At low density in the outer crust these expressions yield ^{56}Fe-nuclei.

According to model I of Oyamatsu (1993), the phase with spherical nuclei in the inner crust is realized up to a density $n_{\text{b}} = 0.0586$ fm^{-3} ($\rho = 0.973\times10^{14}$ g cm^{-3}). This is followed by the phase with rod-like nuclei up to a density $n_{\text{b}} = 0.0749$ fm^{-3} ($\rho = 1.24 \times 10^{14}$ g cm^{-3}), and the phase with slab-like nuclei (up to $n_{\text{b}} = 0.0827$ fm^{-3}, $\rho = 1.37 \times 10^{14}$ g cm^{-3}). Subsequently there are two phases with the roles of nuclear matter and neutron matter reversed, the rod-like one (up to $n_{\text{b}} = 0.0854$ fm^{-3}, $\rho = 1.42\times10^{14}$ g cm^{-3}), and the "Swiss cheese" (inverted-spheres) one, which is the analog of the phase with spherical nuclei and is the last phase in the neutron-star crust (up to $n_{\text{b}} = 0.0861$ fm^{-3}, $\rho = 1.43 \times 10^{14}$ g cm^{-3}). At higher

density the nuclei dissolve to give the uniform matter of the neutron star core.

In each crystalline phase of matter the Wigner–Seitz cell has its own geometry, but we shall assume that in the case of bcc phases it may be approximated by a sphere, and in rod-like phases by a right circular cylinder. We shall assume that the nucleon density distributions may be described by Eq. (12), where r is the distance from the cell center (e.g., from the axis of a rod in the rod-like phase, or from the symmetry plane in the slab-like case). We interpolate these parameters as functions of n_{b} within each phase separately. In the phases with spheres, rods and slabs, $n_{\text{p}}^{\text{out}} = 0$, and $n_{\text{n}}^{\text{out}}$ describes the number density of free neutrons, and the region $r < R_{\text{n}}$ is occupied by the nucleus itself (with $n_{\text{n}}^{\text{in}} > n_{\text{n}}^{\text{out}}$). In the two last "bubble" phases with the roles of nuclear matter and neutron matter reversed, $n_{\text{p}}^{\text{out}} \neq 0$, and $n_j^{\text{out}} > n_j^{\text{in}}$, i.e., the local number density of neutrons and protons increases with distance r from the center of the Wigner–Seitz cell. With increasing density the nucleon density profiles become smoother, approaching that for uniform matter.

Thus we have obtained a simple analytic description of the neutron and proton local density profiles for the ground-state matter throughout the outer and inner neutron-star crusts including non-spherical phases of atomic nuclei. This description will be used below and will be referred to as the *smooth composition* (SC) model of ground-state matter. Using this model one may easily determine the nuclear form factor $F(\boldsymbol{q})$ numerically by calculating the Fourier transform of $n_{\text{p}}(r)$. Unfortunately, vibrational properties are known only for crystals composed of spherical nuclei, apart from recent work on the elastic constants (Pethick & Potekhin 1998). Thus in phases with non-spherical nuclei we know neither the Debye–Waller factor nor the phonon spectrum.

3. General formalism

The general expression for the neutrino emissivity Q due to the neutrino-pair bremsstrahlung (1) of relativistic degenerate electrons in a plasma of spherical nuclei can be written as (Haensel et al. 1996)

$$
\begin{aligned}
Q &= \frac{8\pi G_{\text{F}}^2 Z^2 e^4 C_+^2}{567 \hbar^9 c^8} (k_{\text{B}} T)^6 n_{\text{i}} L \\
&\approx 3.229 \times 10^{11} \rho_{12} \, Z Y_{\text{e}} \, T_8^6 \, L \text{ erg s}^{-1} \text{ cm}^{-3}, \quad (13)
\end{aligned}
$$

where $G_{\text{F}} = 1.436\times10^{-49}$ erg cm^3 is the Fermi weak coupling constant, and L is a dimensionless function to be determined. Furthermore, $C_+^2 = C_V^2 + C_A^2 + 2(C_V'^2 + C_A'^2)$, where C_V and C_A are the vector and axial-vector constants of weak interaction, respectively. We have $C_V = 2\sin^2\theta_{\text{W}} + 0.5$ and $C_A = 0.5$, for the emission of electron neutrinos, to which both charged and neutral currents contribute, and $C_V' = 2\sin^2\theta_{\text{W}} - 0.5$ and $C_A' = -0.5$, for the emission of muonic and tauonic neutrinos, which is due only to neutral currents. In this case, θ_{W} is the Weinberg angle, $\sin^2\theta_{\text{W}} \simeq 0.23$. Eq. (13) with $C_+^2 \approx 1.675$ is obtained taking into account the emission of the three neutrino flavors (ν_{e}, ν_μ, and ν_τ).

Thus the problem reduces to evaluating the function L. In the liquid of atomic nuclei, $L = L_{\mathrm{liq}}$ is determined by the Coulomb scattering of electrons by nuclei (Sect. 3.1). In the Coulomb solid, L consists of two parts,

$$L = L_{\mathrm{sol}} = L_{\mathrm{ph}} + L_{\mathrm{sl}}, \tag{14}$$

where L_{ph} describes the phonon contribution (Sect. 3.2) and L_{sl} describes the static-lattice contribution (Sect. 3.3).

The non-spherical nuclei at the bottom of the neutron-star crust form a liquid crystal at the temperatures of interest. However, since the vibrational properties of these phases are largely unknown, we shall not consider the phonon contribution for this case. The static-lattice contribution for such a solid will be analyzed in Sect. 3.3.

3.1. Liquid phase

The factor L_{liq} is a slowly varying function of the plasma parameters and it has basically the same significance as the Coulomb logarithm in calculations of transport processes in plasmas. The most general expression for it was obtained by Haensel et al. (1996), who found

$$
\begin{aligned}
L_{\mathrm{liq}} =\ & \frac{\hbar c}{k_{\mathrm{B}} T} \int_0^{2k_{\mathrm{F}}} \mathrm{d}q_t\, q_t^3 \int_0^\infty \mathrm{d}q_r\, \frac{S(q)|F(q)|^2}{q^4 |\epsilon(q)|^2} \\
& \times R_T(q_t, q_r)\, R_{\mathrm{NB}}(q_t),
\end{aligned}
\tag{15}
$$

where $\boldsymbol{q} = \boldsymbol{q}_t + \boldsymbol{q}_r$ is the momentum transfer from an electron to a nucleus in a collision event, $\boldsymbol{q}_t$ corresponding to purely elastic Coulomb scattering while $\boldsymbol{q}_r$ takes into account inelasticity due to the neutrino emission; $F(q)$ is the nuclear form factor, $\epsilon(q)$ is the static longitudinal dielectric function (Sect. 2), $S(q)$ is the ion-ion structure factor (e.g., Itoh et al. 1983; Young et al. 1991), and $R_{\mathrm{NB}}(q_t)$ includes non-Born corrections. The function $R_T(q_t, q_r)$ is given by Eq. (20) in Haensel et al. (1996) and describes the effects concerned with the thermal smearing of the electron distribution function.

In the ultra-relativistic limit, the Coulomb logarithm depends actually on three dimensionless parameters: $L_{\mathrm{liq}} = L_{\mathrm{liq}}(Z, \eta, t_{\mathrm{F}})$, $\eta = R_{\mathrm{c}}/a$, $t_{\mathrm{F}} = k_{\mathrm{B}} T/(2 p_{\mathrm{F}} c) \approx T/(2T_{\mathrm{F}})$, where T_{F} is given by Eq. (3).

Haensel et al. (1996) calculated the Coulomb logarithm (15) with the form factor (11) at $Z \le 50$, $t_{\mathrm{F}} \lesssim 0.1$ and $\eta \lesssim 0.2$ and fitted the results by an analytic formula (their Eq. (25)). In this article, we shall calculate L_{liq} from the starting equation (15) since we shall not restrict ourselves to the simple form factor (11) (Sect. 2). We shall use the structure factor $S(q)$ obtained by Rogers & DeWitt (unpublished) and accurately fitted by Young et al. (1991).

Notice that if we neglect the thermal smearing of the electron distribution, then Eq. (15) reduces to the familiar expression (e.g., Festa & Ruderman 1969)

$$L_{\mathrm{liq}} = \int_0^1 \mathrm{d}y\, \frac{S(q)|F(q)|^2}{y|\epsilon(q)|^2}\left(1 + \frac{2y^2}{1 - y^2}\ln y\right) R_{\mathrm{NB}}(q), \tag{16}$$

where $y = q/(2k_{\mathrm{F}})$. As shown by Haensel et al. (1996), it is a good approximation for $T \ll \hbar c q_{\mathrm{s}}$, where $q_{\mathrm{s}} \sim a^{-1}$ is the Coulomb screening momentum.

The factor $R_{\mathrm{NB}}(q)$ represents (Haensel et al. 1996) the ratio of the electron scattering cross sections by atomic nucleus calculated exactly and in the Born approximation. It describes the non-Born correction to the Born approximation. To simplify consideration of the non-Born corrections we have introduced the mean non-Born correction factor $\bar{R}_{\mathrm{NB}}$ defined as

$$\bar{R}_{\mathrm{NB}} = L_{\mathrm{liq}}^{\mathrm{NB}} / L_{\mathrm{liq}}^{\mathrm{Born}}, \tag{17}$$

where $L_{\mathrm{liq}}^{\mathrm{NB}}$ and $L_{\mathrm{liq}}^{\mathrm{Born}}$ are given by Eq. (15) calculated with an accurate factor R_{NB} and with $R_{\mathrm{NB}} = 1$, respectively. We have evaluated $\bar{R}_{\mathrm{NB}}$ using the form factor (11) for wide ranges of the parameters Z, η, t_{F} (or Γ) typical for neutron star envelopes. $\bar{R}_{\mathrm{NB}}$ appears to be a very slow function of η and Γ. Since our treatment of the non-Born corrections is rather phenomenological anyway, we have set $\Gamma = 150$ and $\eta = 0.1$ and neglected the thermal smearing of the electron distribution function. Then $\bar{R}_{\mathrm{NB}}$ is a function of the only remaining parameter, Z. The numerical results for $Z \lesssim 60$ are accurately fitted by

$$\bar{R}_{\mathrm{NB}} = 1 + 0.00554\, Z + 0.0000737\, Z^2. \tag{18}$$

This formula enables us to calculate L_{liq} from Eq. (15) or (16) with $R_{\mathrm{NB}}(q) = 1$, i.e., in the Born approximation, and introduce the mean non-Born correction (18) using Eq. (17).

An accurate calculation of the non-Born corrections in crystalline matter (Sects. 3.2 and 3.3) is a difficult task which goes beyond the scope of the present paper. However, we shall see (Sect. 4) that neutrino bremsstrahlung in crystalline matter is quite similar to that in a Coulomb liquid. Thus we adopt the same factor (18) to account for the non-Born corrections in Coulomb crystals.

3.2. Phonon contribution

The phonon contribution in a Coulomb crystal of spherical nuclei was studied by a number of authors (e.g., Flowers 1973; Itoh et al. 1984b; Yakovlev & Kaminker 1996). So far, all articles have been restricted to consideration of one-phonon processes (absorption or emission of one phonon). To allow for the background lattice vibrations the one-phonon reaction rate has usually been multiplied by e^{-2W}, where $W = W(q)$ is the Debye–Waller factor introduced in Eq. (8).

Under astrophysical conditions at not too low temperatures, the main contribution to electron–phonon scattering comes from *umklapp* processes, in which the electron momentum transfer $\hbar\boldsymbol{q}$ in a scattering event lies outside the first Brillouin zone. Then the phonon (quasi)momentum is determined by reduction of $\boldsymbol{q}$ to the first Brillouin zone. The umklapp processes require $q \gtrsim q_0$, contrary to the normal processes in which $\boldsymbol{q}$ remains in the first Brillouin zone and $q \lesssim q_0$, where $q_0 \approx (6\pi^2 n_{\mathrm{i}})^{1/3}$ is the radius of the Brillouin zone in the approximation in which it is treated as a sphere. Umklapp processes dominate since the parameter $y_0 = q_0/(2k_{\mathrm{F}}) = (4Z)^{-1/3}$ is typically small (due to the large Z). Accordingly the phase space associated with

umklapp processes is much larger than that for the normal ones (e.g., Raikh & Yakovlev 1982) and, in most cases, it is sufficient to consider umklapp processes alone.

Let us rederive the expression for L_{ph} with a proper treatment of multi-phonon processes. We start from the general integral expression (Eq. (18) of Flowers 1973) for the neutrino emissivity due to electron-phonon scattering. The integrand contains the inelastic part $S_{\mathrm{d}}(q, \Omega)$ of the dynamical structure factor of ions in a Coulomb crystal. It is the inelastic part that is responsible for the electron-phonon scattering. Baiko et al. (1998) have obtained its expression for $q \gtrsim q_0$ by accurate summation of multi-phonon diagrams:

$$S_{\mathrm{d}}(q, \Omega) = \int_{-\infty}^{+\infty} dt\, e^{i\Omega t}\, S(q, t),$$
$$S(q, t) = e^{-2W} \left(e^{\Phi(t)} - 1 \right), \tag{19}$$

where

$$\Phi(t) = \frac{\hbar q^2}{2 m_{\mathrm{i}}} \left\langle \frac{\cos\left[\omega_s (t + i\hbar/2k_{\mathrm{B}}T)\right]}{\omega_s \sinh\left(\hbar\omega_s/2k_{\mathrm{B}}T\right)} \right\rangle. \tag{20}$$

In these calculations the density operators are calculated to all orders in the phonon creation and annihilation operators, but the phonon dynamics is treated in the harmonic approximation.

We now use the approach of Flowers (1973) with the dynamical structure factor (19) and make the same simplifications as in deriving the expression for L_{ph} by a semianalytical method described by Yakovlev & Kaminker (1996). Then we obtain

$$L_{\mathrm{ph}} = \int_{y_0}^{1} dy\, \frac{S_{\mathrm{eff}}(q)|F(q)|^2}{y|\epsilon(q)|^2} \left(1 + \frac{2y^2}{1 - y^2} \ln y\right). \tag{21}$$

In this case

$$S_{\mathrm{eff}}(q) = \frac{63\hbar^6}{16\pi^7 (k_{\mathrm{B}}T)^6} \int_0^\infty d\omega\, \omega^4 \int_{-\infty}^{+\infty} d\Omega \int_{-\infty}^{+\infty} dt$$
$$\times \frac{\Omega + \omega}{e^{\hbar(\Omega+\omega)/k_{\mathrm{B}}T} - 1}\, e^{i\Omega t} S(q, t), \tag{22}$$

where $\hbar\omega$ is the neutrino-pair energy. As in Yakovlev & Kaminker (1996) the lower integration limit y_0 excludes the low-momentum transfers in which the umklapp processes are forbidden.

Comparing Eqs. (21) and (16) we see that $S_{\mathrm{eff}}(q)$ plays the role of an effective static structure factor that defines the phonon contribution to the neutrino bremsstrahlung. The expression (22) for it can be easily simplified. First we can integrate over Ω and ω which leaves us with a single integration over t:

$$S_{\mathrm{eff}}(q) = -\frac{189}{2\pi^5} \left(\frac{\hbar}{k_{\mathrm{B}}T}\right)^4 e^{-2W}$$
$$\times \mathrm{Im} \int_{-\infty}^{+\infty} dt\, \frac{e^{\Phi(t)} - 1}{t^5 \sinh^2(\pi t k_{\mathrm{B}}T/\hbar)}. \tag{23}$$

The latter integration is non-trivial since the integrand is singular at $t = 0$. However, the singularity is easily removed by using the theory of functions of a complex variable. Since the function

$\Phi(t)$ is analytic, the integrand allows us to shift the integration path into the complex t plane. The appropriate shift is $t = t' - i\hbar/(2k_{\mathrm{B}}T)$. It transforms Eq. (23) into a rapidly converging integral

$$S_{\mathrm{eff}}(q) = 189 \left(\frac{2}{\pi}\right)^5 e^{-2W} \int_0^\infty d\xi\, \frac{1 - 40\xi^2 + 80\xi^4}{(1 + 4\xi^2)^5 \cosh^2(\pi\xi)}$$
$$\times \left(e^{\Phi(\xi)} - 1\right), \tag{24}$$

where $\xi = t' k_{\mathrm{B}}T/\hbar$ and

$$\Phi(\xi) = \frac{\hbar q^2}{2 m_{\mathrm{i}}} \left\langle \frac{\cos(\omega_s t')}{\omega_s \sinh\left(\hbar\omega_s/2k_{\mathrm{B}}T\right)} \right\rangle. \tag{25}$$

The phonon averaging $\langle \ldots \rangle$ can be performed using the method of Mochkovitch & Hansen (1979). Afterwards the integral (24) can be calculated numerically. The behaviour of $S_{\mathrm{eff}}(q)$ depends on temperature, and may be characterized by the dimensionless parameter $t_{\mathrm{p}} = T/T_{\mathrm{p}}$ introduced in Eq. (9). First consider the asymptotes for $t_{\mathrm{p}} \ll 1$ and $t_{\mathrm{p}} \gtrsim 1$.

In the low-temperature case, $t_{\mathrm{p}} \ll 1$, it is sufficient to set $e^\Phi - 1 = \Phi$ in Eqs. (19), (22) or (24). This case corresponds to the familiar one-phonon approximation adopted in previous articles. In the notation introduced by Yakovlev & Kaminker (1996) one finds in this case that

$$S_{\mathrm{eff}}^{1\mathrm{ph}}(q) = \alpha_0\, y^2\, t_{\mathrm{p}}\, G(t_{\mathrm{p}})\, e^{-2W} \approx \alpha_0\, y^2\, b\, t_{\mathrm{p}}^2\, e^{-2W}, \tag{26}$$

where α_0 is defined in Eq. (10), $G(t_{\mathrm{p}})$ is the function determined by Eq. (12) in Yakovlev & Kaminker (1996), and b is a numerical factor specified by the low-temperature asymptote $G(t_{\mathrm{p}}) = b\, t_{\mathrm{p}}$. For a bcc Coulomb crystal, one has $b \approx 231$. This value is more accurate than $b \approx 202$ given by the numerical fit (15) in Yakovlev & Kaminker (1996) since the latter authors did not intend to produce a fitting formula which would be highly accurate for $t_{\mathrm{p}} \lesssim 0.01$.

Therefore, the results obtained in the previous articles are strictly valid for $T \ll T_{\mathrm{p}}$. The Debye–Waller exponent e^{-2W} included into the one-phonon approximation takes into account renormalization of the one-phonon interaction by background lattice vibrations. Notice that recent calculations of $G(t_{\mathrm{p}})$ in Yakovlev & Kaminker (1996) for the fcc lattice are inaccurate due to an error in specifying the boundaries of the first Brillouin zone (Sect. 2). After correcting this error, we obtain a result for $G(t_{\mathrm{p}})$ very close to that for the bcc lattice. Note also a misprint in Eq. (18) for the function F_1 in Yakovlev & Kaminker (1996): in the second term $(1.5 + \alpha)^{3/4}$ is erroneously printed instead of $(1 + \alpha)^{3/4}$ although all calculations were made using the correct expression.

In the opposite case of high temperatures, $t_{\mathrm{p}} \gtrsim 1$, the asymptotic form of Eq. (24) is very simple,

$$S_{\mathrm{eff}}(q) = 1 - e^{-2W}. \tag{27}$$

Thus $S_{\mathrm{eff}}(q)$ becomes noticeably larger than in the one-phonon approximation, as a result of multi-phonon processes.

We have also calculated $S_{\mathrm{eff}}(q)$ for a wide range of temperatures T and density parameters α_0 defined in Eq. (10). We
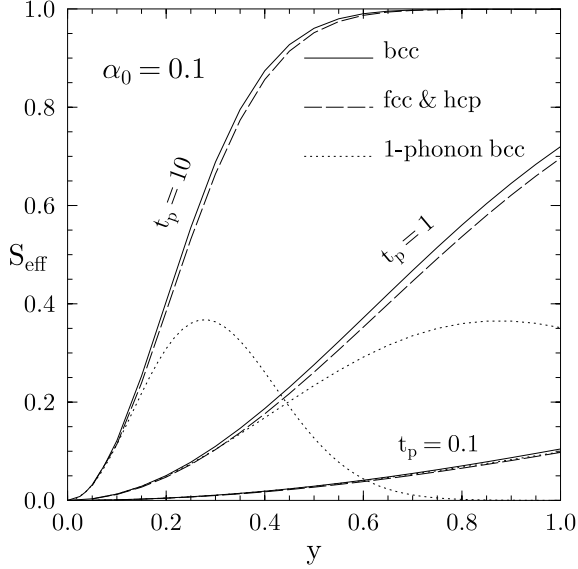
Fig. 2. The effective structure factor $S_{\text{eff}}(q)$ which enters the normalized neutrino emissivity (21), produced by the electron-phonon scattering, for the density parameter $\alpha_0 = 0.1$ and three temperatures $t_{\text{p}} = 0.1, 1, 10$ in bcc, fcc and hcp lattices. The curves for fcc and hcp crystals almost coincide. Dots show the effective structure factor which corresponds to the one-phonon approximation

have verified that, under the conditions in a neutron-star crust, $\alpha_0 \lesssim 0.2$. For such α_0 and all t_{p} the numerical results are fitted by a simple expression

$$S_{\text{eff}}(q) = \left(e^{2W_1} - 1\right) e^{-2W}, \tag{28}$$

where

$$W_1 = \frac{\alpha_0 y^2 b u_{-2} t_{\text{p}}^2}{2 \sqrt{(b t_{\text{p}})^2 + u_{-2}^2 \exp(-7.6 t_{\text{p}})}}, \tag{29}$$

and $b \approx 231$, for a bcc lattice. Notice that $W_1 \approx W \approx 0.5 \alpha_0 y^2 u_{-2} t_{\text{p}}$ for $t_{\text{p}} \gtrsim 1$. Notice also that $S_{\text{eff}}(q)$ given by Eq. (28) reproduces quite accurately $S_{\text{eff}}^{\text{1ph}}(q)$ if we replace $e^{2W_1} - 1$ by $2W_1$. The effect of multi-phonon processes on neutrino bremsstrahlung emission will be described in Sect. 4.

Fig. 2 shows the dependence of $S_{\text{eff}}(q)$ on y at $\alpha_0 = 0.1$ and three temperatures $t_{\text{p}} = 0.1, 1$, and 10 for three types of Coulomb crystals, bcc, fcc, and hcp. The results are seen to be almost independent of lattice type, and the curves for fcc and hcp lattices are indistinguishable. If $t_{\text{p}} \gtrsim 1$, the one-phonon approximation appears to be highly inaccurate for $y \gtrsim 0.4$.

Note that the present treatment of phonon scattering is valid as long as $T \gtrsim T_{\text{u}}$, where $T_{\text{u}} \sim T_{\text{p}} Z^{1/3} e^2/(\hbar v_{\text{F}})$ is the temperature below which umklapp processes are frozen out (see, e.g., Raikh & Yakovlev 1982), and $v_{\text{F}} \approx c$ is the electron Fermi velocity. If $T \gtrsim T_{\text{u}}$ the electron–phonon scattering can be described in the free electron approximation, and the main contribution to the scattering comes from umklapp processes (Yakovlev & Urpin 1980; Raikh & Yakovlev 1982). The density dependence of T_{u} is shown in Fig. 1 of the article by Baiko &

Yakovlev (1996); T_{u} is so low that a study of neutrino emission at lower temperatures is of no practical importance.

3.3. Static-lattice contribution

This contribution corresponds to neutrino emission due to Bragg diffraction of electrons in a crystal. It was widely assumed for a long time that the process could be studied in the free-electron approximation (e.g., Flowers 1973; Itoh et al. 1984a). However, recently Pethick & Thorsson (1994) have pointed out the importance of electron band-structure effects. The gaps in the electron dispersion relation at the boundaries of the Brillouin zones can reduce noticeably the static-lattice contribution as compared to that obtained in the free-electron approximation. The general formalism for evaluating the static-lattice contribution for strongly degenerate relativistic electrons with proper treatment of band-structure effects has been developed by Pethick & Thorsson (1997). Their Eq. (28) is valid for spherical and nonspherical nuclei and can be written as

$$
\begin{aligned}
Q_{\text{sl}} &= \frac{2\pi G_{\text{F}}^2 k_{\text{F}} C_+^2}{567 \hbar^9 c^8} (k_{\text{B}}T)^8 J \\
&\approx 1.254 \times 10^9 \, (\rho_{12} Y_{\text{e}})^{1/3} T_8^8 \, J \text{ erg s}^{-1} \text{ cm}^{-3},
\end{aligned} \tag{30}
$$

where

$$J = \sum_{\boldsymbol{K} \neq 0} \frac{y^2}{t_V^2} I(y, t_V) \tag{31}$$

is a dimensionless function given by a sum over all reciprocal lattice vectors $\boldsymbol{K} \neq 0$ for which $\boldsymbol{K}/2$ lies within the electron Fermi surface; $y = K/(2k_{\text{F}})$ (with $y < 1$). The function $I(y, t_V)$ is given by Eq. (29) in Pethick & Thorsson (1997), which can be rewritten as

$$
\begin{aligned}
I(y, t_V) &= \frac{63}{8\pi^7} \frac{y}{y_\perp^4} \int_0^\infty \int_0^\infty \frac{dz_1 \, dz_2}{E_1 E_2} \int_{w_1}^{w_2} dw \frac{w^2}{e^w - 1} \\
&\quad \times [(w_2 - w)(w - w_1)]^{3/2},
\end{aligned} \tag{32}
$$

where $y_\perp = \sqrt{1 - y^2}$,

$$E_{1,2} = \sqrt{1 + \left(z_1 \mp \frac{z_2}{2}\right)^2},$$

$$w_{1,2} = \frac{E_1 + E_2 \mp y_\perp \sqrt{(E_1 + E_2)^2 - z_2^2}}{t_V y^2}; \tag{33}$$

t_V is defined in terms of the Fourier transform of the lattice potential (7) with $\boldsymbol{q} = \boldsymbol{K}$ by

$$\frac{1}{t_V} = \frac{|V_{\boldsymbol{K}}| y_\perp}{k_{\text{B}}T} = \frac{4\pi e \rho_Z}{K^2 k_{\text{B}}T} \frac{|F(K)|}{|\epsilon(K)|} y_\perp \, e^{-W(K)}, \tag{34}$$

and other notations were introduced in Eq. (7).

For a lattice of spherical nuclei, we can use Eq. (13) with

$$
\begin{aligned}
L_{\text{sl}} &= \frac{\pi Z^2}{3\Gamma^2} (9\pi Z/4)^{1/3} J \\
&= \frac{1}{12Z} \sum_{\boldsymbol{K} \neq 0} \frac{y_\perp^2}{y^2} \frac{|F(K)|^2}{|\epsilon(K)|^2} I(y, t_V) \, e^{-2W(K)}.
\end{aligned} \tag{35}
$$

According to Eqs. (9), (34) and (35), the Debye–Waller factor suppresses the electron–lattice interaction at large reciprocal lattice vectors $\boldsymbol{K}$ and weakens the neutrino emission. Computing Q_{sl} directly as a sum of 3D integrals (32) is time consuming since the number of reciprocal lattice vectors $\boldsymbol{K}$ involved is generally large ($\sim 4Z$ terms). We simplify computation by producing an analytic fit to $I(y, t_V)$.

Analytical asymptotes of $I(y, t_V)$ can be derived in the limiting cases of high and low temperatures. In the high-temperature limit, $t_V \gg 1$, Pethick & Thorsson (1994, 1997) obtained

$$I = \frac{1}{y_\perp^2 y}\left(1 + \frac{2\,y^2}{y_\perp^2}\ln y\right). \tag{36}$$

Inserting this asymptote into Eqs. (35) and (13) one immediately reproduces the well-known result of Flowers (1973) and Itoh et al. (1984a) for the static-lattice contribution when band-structure effects are neglected. Replacing the sum over $\boldsymbol{K}$ by an integral over q, we arrive at the expression

$$L_{sl}^{(0)} = \int_{y_0}^{1} \mathrm{d}y\, \frac{|F(q)|^2 \mathrm{e}^{-2W}}{y|\epsilon(q)|^2}\left(1 + \frac{2y^2}{1 - y^2}\ln y\right), \tag{37}$$

which is similar to Eqs. (16) and (21) in the liquid and for the phonon contribution in the solid, respectively. The Debye–Waller exponent e^{-2W} is seen to play the role of the diffraction part of an "effective static structure factor" that defines the static-lattice contribution (smoothed over diffraction peaks due to replacing summation by integration). Thus the sum $L_{ph} + L_{sl}^{(0)}$ in a crystal can be written in the same form (16) as L_{liq} in a liquid, with an effective structure factor $S_{sol}(q) = \mathrm{e}^{-2W} + S_{eff}(q)$. We have verified that $S_{sol}(q)$ resembles the structure factor $S(q)$ in a strongly coupled liquid (Young et al. 1991) for ion coupling parameters $100 \lesssim \Gamma \lesssim 225$ if we smear out the familiar diffraction peaks in $S(q)$; the integral contributions of the two factors are nearly the same. This elucidates the similarity of neutrino-pair bremsstrahlung in a liquid and a crystal (Sect. 4).

The asymptote (36) is temperature-independent. The lowest-order thermal correction can be taken into account by introducing the factor $[1 + (63/40)(\pi t_V y)^{-2}]$.

The low-temperature asymptote for $t_V \ll y_\perp/y^2$ is (Pethick & Thorsson 1997)

$$
\begin{aligned}
I(y, t_V) = {} & \frac{189}{2\pi^{11/2}(1 - y_\perp)^{1/2}(1 + y_\perp)^2(y_\perp t_V)^{5/2}} \\
& \times \exp\left(-\frac{2}{t_V(1 + y_\perp)}\right),
\end{aligned}
\tag{38}
$$

while for $y_\perp/y^2 \ll t_V \ll 1$ the latter asymptote has to be multiplied by $\sqrt{\pi}[y_\perp/(t_V y^2)]^{5/2}$.

We calculated $I(y, t_V)$ from Eq. (32) numerically for wide ranges of y and t_V and derived an analytic fit which reproduces numerical results and the asymptotes:

$$
\begin{aligned}
I(y, t_V) = {} & \frac{0.3088\,(1 + 8.416 y_\perp t_V)}{y\,(1 + y_\perp)^{3/2}\,(y_\perp t_V)^{5/2}\,D}\exp\left[-\frac{2}{t_V(1 + y_\perp)}\right] \\
& + \frac{1}{y_\perp^2 y}\left(1 + \frac{0.4031}{t_V^2 y^2 + 0.5 t_V + 0.2678}\right)
\end{aligned}
$$

$$\times\left(1 + \frac{2y^2}{y_\perp^2}\ln y\right)\exp\left(-\frac{2}{t_V H}\right), \tag{39}$$

where $D = u^5 + 0.7124\,u^4 - 1.689\,u^3 + 5.237\,u^2 - 0.2\,u + 1.772$, $H = 1 + y_\perp + 8.212\,t_V y^2$, and $u = y\sqrt{t_V/y_\perp}$. The mean error of the fit is 2%, and the maximum error of 7.4% occurs at $t_V = 0.045$ and $y = 0.987$. The fit permits a rapid and accurate evaluation of the static-lattice contribution from Eqs. (30) and (31) or (13) and (35) for any plasma parameters of practical interest.

For a lattice of spherical nuclei, we can use Eq. (35) with the Debye–Waller factor and the nuclear form factor, and calculate the sum over reciprocal lattice vectors for bcc, fcc and hcp crystals. In the case of non-spherical nuclei, we use the more general Eqs. (30) and (31) including the form factor but setting $W = 0$, since the Debye–Waller factor is unknown. The sum over reciprocal lattice vectors in Eq. (31) for a lattice of non-spherical nuclei is different from that for ordinary crystals. In the case of rod-like phases, the lattice is the simplest two-dimensional triangular one, for slab-like nuclei the lattice is purely one-dimensional, and in the case of the Swiss-cheese phase with neutron drops immersed in nuclear matter we shall assume that the lattice is bcc.

4. Results and discussion

Let us outline the main properties of neutrino-pair bremsstrahlung by relativistic degenerate electrons in neutron-star crusts. The results of Sect. 3 allow us to calculate the neutrino emission for bcc, fcc and hcp Coulomb crystals of atomic nuclei. However, in all three cases the emission appears to be practically the same because of the close similarity of the crystals. For simplicity we therefore consider bcc crystals throughout this section.

Figs. 3 and 4 show the temperature dependence of the normalized neutrino emissivity L for two densities, $\rho = 10^{10}$ and $10^{12}\,\mathrm{g\,cm^{-3}}$, in the outer and inner crusts, respectively. Fig. 3 is plotted for matter composed of iron ($Z = 26$, $A = 56$), while Fig. 4 corresponds to the ground-state matter composed of $^{250}_{40}\mathrm{Zr}$ nuclei ($Z = 40$, $A = 250$, where A is the number of nucleons per Wigner–Seitz cell, see Negele & Vautherin 1973). Vertical dotted lines separate liquid and solid phases. The upper (dashed) line in the liquid phase is obtained from Eq. (15) with the non-Born corrections included in the function R_{NB} (Haensel et al., 1996). The lower (solid) line is also obtained from Eq. (15) but in the Born approximation ($R_{NB} = 1$). Solid lines in the crystalline phase show the phonon contribution (Sect. 3.2), the static-lattice contribution (Sect. 3.3), and the total function L_{sol} given by Eq. (14). The dotted line also gives the total function but neglecting the band structure effects in the static-lattice contribution (by using the asymptote (36) in Eq. (35)). Finally, the dot-dashed line displays the phonon contribution calculated in the one-phonon approximation adopted in previous articles (Sect. 3.2).

The temperature profiles of L in Figs. 3 and 4 are similar. The phonon contribution is generally several times smaller than the static-lattice one. Each term in the static-lattice sum
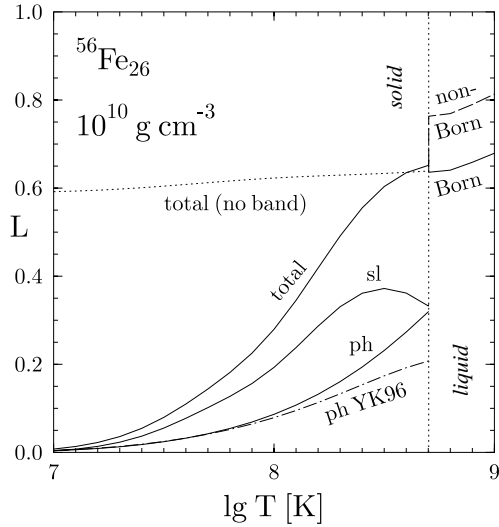
Fig. 3. Temperature dependence of the normalized neutrino emissivity L for iron matter at $\rho = 10^{10}\,\mathrm{g\,cm^{-3}}$. Solid lines: Born results for the liquid phase; phonon and static-lattice contributions, as well as the total function (14) for the crystalline phase. Dotted line: the total function for crystalline phase but without band-structure effects. Dashed line: non-Born result in the liquid phase. Dot-dashed line: one-phonon approximation for the phonon contribution (Yakovlev & Kaminker 1996). All curves but one in the liquid phase are obtained in the Born approximation
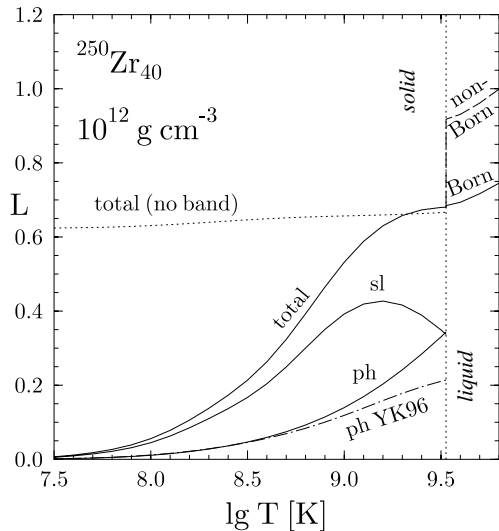
Fig. 4. Same as in Fig. 3 but for ground-state matter composed of $^{250}_{40}\mathrm{Zr}$ nuclei at $\rho = 10^{12}\,\mathrm{g\,cm^{-3}}$

(35) is suppressed exponentially with decreasing temperature but the sum itself decreases more like a power law because, for the smallest reciprocal lattice vectors $|\boldsymbol{K}|$, the exponential decrease of the contribution starts to operate at much higher temperature than that for larger reciprocal lattice vectors (Pethick & Thorsson 1997). At very low temperatures, the reduction of contributions from all reciprocal lattice vectors becomes exponential, and the total static-lattice contribution is suppressed exponentially. However, such low temperatures are of no practical importance. Generally, the static-lattice neutrino emission is

usually partially suppressed by band-structure effects, and these effects are substantial.

All calculations of neutrino-pair emission in the crystalline phase have been made in the Born approximation. On the other hand, Haensel et al. (1996) calculated L_{liq} beyond the Born approximation. For comparison of the results in the crystalline and liquid phases, we present also the Coulomb logarithm L_{liq} determined in the Born approximation. This curve matches the function L_{sol} in the solid phase much better and makes L an almost continuous function of temperature at the melting point. We believe that the non-Born curve in the solid phase (which is difficult to calculate exactly) would match equally well the non-Born curve in the liquid phase, because of the similarity of the bremsstrahlung in a liquid and in a crystal, mentioned in Sect. 3.3. The state of a Coulomb system (liquid or solid) is expected to have little effect on neutrino-bremsstrahlung, since in both cases neutrino emission occurs due to scattering of electrons by fluctuations of electric charge produced by ions (nuclei). In the solid phase near the melting point both the phonon and the static-lattice contributions must be included for the total emission rate to match the results in the liquid phase. The one-phonon approximation is seen to be generally quite accurate at low temperatures, $T \ll T_{\mathrm{m}}$ (actually at $T \ll T_{\mathrm{p}}$, as discussed in Sect. 3.2) but underestimates the phonon contribution near the melting point. It is the proper inclusion of multi-phonon processes that makes the phonon contribution larger and almost removes the jump of the total neutrino emissivity at the melting point. Notice that the phonon and static-lattice contributions at the melting become nearly equal. The physical properties of a Coulomb liquid and a Coulomb solid near the melting point are nearly the same. To verify this statement we have shifted artificially the melting temperature (which actually corresponds to $\Gamma = \Gamma_{\mathrm{m}} = 172$, Sect. 2). We have considered the cases of a supercooled liquid by taking $\Gamma_{\mathrm{m}} = 225$, for which the liquid-state structure factors of Young et al. (1991) are available, and the case of a superheated crystal by taking $\Gamma_{\mathrm{m}} = 100$. In all the cases the total normalized neutrino emissivities L do not differ noticeably from those obtained at $\Gamma_{\mathrm{m}} = 172$, and the discontinuity of L at the melting point is minor.

Fig. 5 compares the present results for $^{56}\mathrm{Fe}$ matter at $\rho = 10^9\,\mathrm{g\,cm^{-3}}$ with the familiar results by N. Itoh and his group reviewed recently by Itoh et al. (1996) and with the results by Yakovlev & Kaminker (1996) for the phonon contribution obtained in the one-phonon approximation.[1] The temperatures displayed are rather low, so the one-phonon approximation almost coincides with the multi-phonon calculation. One can see a transition from power-law to exponential decrease in our static-lattice curve with decreasing temperature at $T \sim 10^7$ K. For

---

[1] Note that Yakovlev & Kaminker (1996), while comparing their results for the one-phonon contribution in the iron and carbon plasmas at $\rho = 10^9\,\mathrm{g\,cm^{-3}}$ (their Figs. 3 and 4) with the results of Itoh et al. (1996), inaccurately plotted (by long dashes) the fit expressions of Itoh et al. (1996). The correct curves are closer to the results by Yakovlev & Kaminker (1996) and are plotted in the present Figs. 5 and 6. Two of the authors (DY and AK) are grateful to Prof. N. Itoh for pointing out this omission.
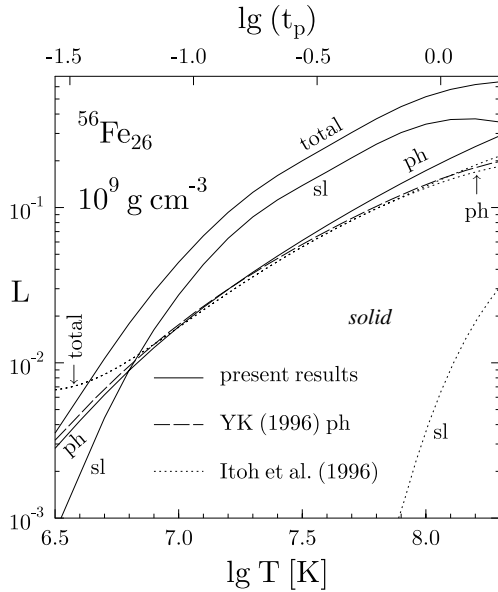
Fig. 5. Phonon (ph), static-lattice (sl) and total normalized neutrino emissivities L_{ph}, L_{sl}, L_{sol} vs T (lower horizontal scale) or t_p (upper horizontal scale) for a crystal of ^{56}Fe nuclei at $\rho = 10^9$ g cm^{-3} calculated in the Born approximation. Solid curves show the present results, dashes show the phonon contribution in the one-phonon approximation (Yakovlev & Kaminker 1996) while dots are the results of Itoh et al. (1996)

lower T, the phonon contribution dominates over the static-lattice one. The static-lattice contribution given by Itoh et al. (1996) is underestimated by several orders of magnitude. The authors calculated this contribution neglecting the electron band structure and multiplied this result by a factor which should approximately take into account the suppression of the neutrino emission due to band structure. The latter factor was chosen on the assumption that one particular reciprocal lattice vector gave the dominant contribution at all temperatures. If this were the case, the suppression would be exponential. However, as shown above, the suppression of contributions from the various reciprocal lattice vectors sets in at different temperatures, and the resulting suppression of the total rate is much weaker than given by the approximation of Itoh et al. (1996). In fact, the approximate suppression factor introduced by Itoh et al. (1996) makes the static-lattice contribution negligible at all densities and temperatures of practical interest. Since the actual static-lattice emission is commonly several times larger than the phonon one, the approach of Itoh et al. (1996) systematically underestimates the total neutrino emissivity in the solid phase of dense matter. In addition, the phonon contribution given by Itoh et al. (1996) appears to be overestimated for $T \lesssim 10^7$ K (Fig. 5) as a result of the analytic fits proposed by Itoh et al. (1996) being insufficiently accurate (Yakovlev & Kaminker 1996).

Fig. 6 presents a similar comparison of the results but for carbon. The case of carbon at high density is extreme since zero-point vibrations of the light carbon ions become very strong. Nuclear reactions and beta captures tend to transform carbon into heavier elements. The Debye–Waller factor is very large
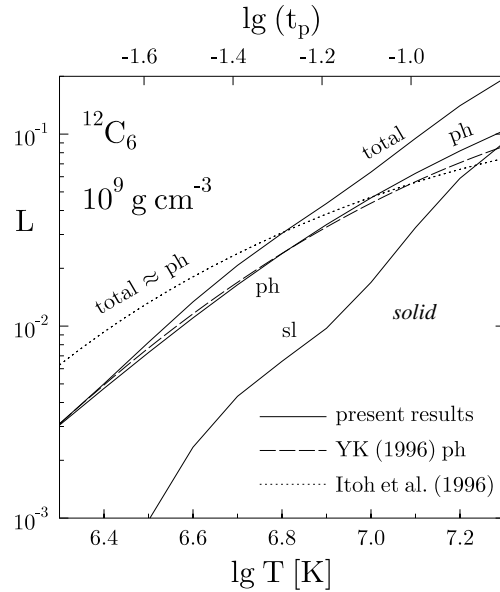

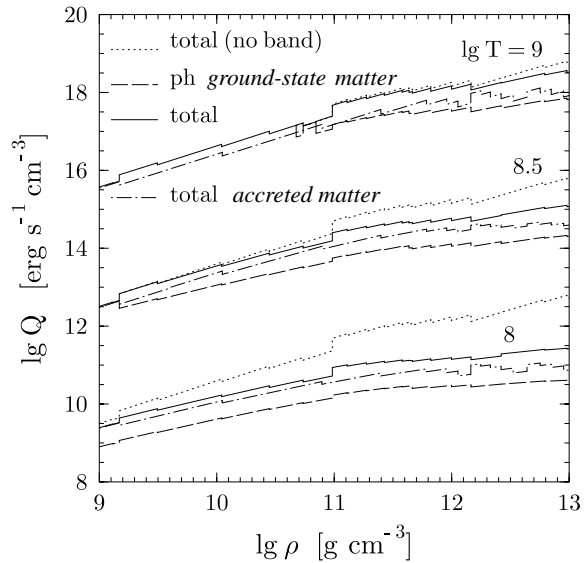**Fig. 6.** Same as in Fig. 5 but for carbon crystal

Fig. 7. Density dependence of the neutrino bremsstrahlung emissivity at $T = 10^8$, $10^{8.5}$ and 10^9 K for ground-state and accreted matter calculated with the form factor (11). Solid and dashed lines show the total and phonon emissivities, respectively, for ground-state matter; dots present the same total emissivity but obtained neglecting the electron band-structure effects. Dot-dashed lines display the total emissivity for accreted matter

owing to zero-point vibrations ($\alpha \propto u_{-1}/\sqrt{A_i Z}$ at $t_p \ll 1$, see Eq. (9)). It suppresses drastically the static-lattice contribution and makes it generally smaller than the phonon contribution. The simplified treatment of the band-structure effects by Itoh et al. (1996) damps the static-lattice contribution especially strongly, by several orders of magnitude, making $L_{sol} \approx L_{ph}$.

Fig. 7 shows the density dependence (10^9 g cm$^{-3} \leq \rho \leq 10^{13}$ g cm^{-3}) of the neutrino emissivity at three values of T for the ground-state and accreted matter. Here and in all subsequent

figures the emissivities are calculated in the Born approximation and multiplied by the non-Born correction factor (18) as discussed in Sect. 3.1. Note that self-consistent models of accreted matter (e.g., Miralda-Escudé et al. 1990) correspond to $T \sim 10^8$ K. We use the accreted model for higher T to illustrate how variations of nuclear composition affect the neutrino emission. For a particular temperature and density, matter will be either liquid or solid. In the liquid state, we calculate Q using Eq. (15). In the solid state, we present the total and phonon neutrino emissivities for ground-state matter and the total emissivity for the accreted matter. In accreted matter the ratio of the total emissivity to the phonon one is qualitatively the same as in ground-state matter. We show also the total neutrino emissivity for ground-state matter neglecting band-structure effects. In the displayed density range, matter is entirely solid for $T = 10^8$ K; there is one melting point for $T = 10^{8.5}$ K ($\lg \rho_{\rm m}$ [g cm^{-3}] = 9.17, for ground-state matter) which separates liquid (at $\rho < \rho_{\rm m}$) and solid (at $\rho > \rho_{\rm m}$); and there is a series of melting points at $T = 10^9$ K due to the non-monotonic behaviour of the melting curves $T_{\rm m} = T_{\rm m}(\rho)$ associated with strong variations of the nuclear composition. The positions of the melting points can be deduced from Fig. 1. For ground-state matter, these positions can also be traced in Fig. 7 from the appearance of the phonon contribution (dashed lines). With decreasing temperature the solidification front shifts toward lower densities. The accreted matter solidifies at higher densities than does ground-state matter due to the lower atomic number. At the melting points the neutrino emissivities exhibit some jumps, but these are small because, as we remarked earlier, neutrino bremsstrahlung does not change qualitatively while passing from liquid to solid matter. Other, stronger jumps are associated with variations of the nuclear composition (Sect. 2). Notice that the jumps of both types may be ignored in practical applications. The reduction of the neutrino emission by the band-structure effects becomes stronger with decreasing temperature and reaches one order of magnitude for $T \sim 10^8$ K and $\rho \gtrsim 10^{11}$ g cm^{-3}. The band-structure reduction is power-law (non-exponential) for the parameters displayed in Fig. 7. The ratio of the phonon contribution to the static-lattice one remains nearly constant for a wide range of temperatures much below the melting temperature, and the static-lattice contribution is several times larger than the phonon one. The neutrino bremsstrahlung in the accreted matter is lower than in the ground-state matter due to the lower atomic number, but the difference is not large.

The effects of various physical factors on the density dependence of the bremsstrahlung emissivity in the lattice of ground-state matter at $T = 3 \times 10^8$ K is shown in Fig. 8. We present the total emissivity, and also the static-lattice and phonon emissivities. In addition, we show the total emissivity calculated neglecting either the effects of band-structure, the Debye–Waller factor, or the nuclear form factor. Here by the phrase "neglecting the Debye–Waller factor" we mean the one-phonon approximation in which the Debye–Waller factor is set to zero. One can see that the phonon contribution is noticeably smaller than the static-lattice one, and the ratio of the static-lattice and phonon contributions increases slowly with density, reaching a factor
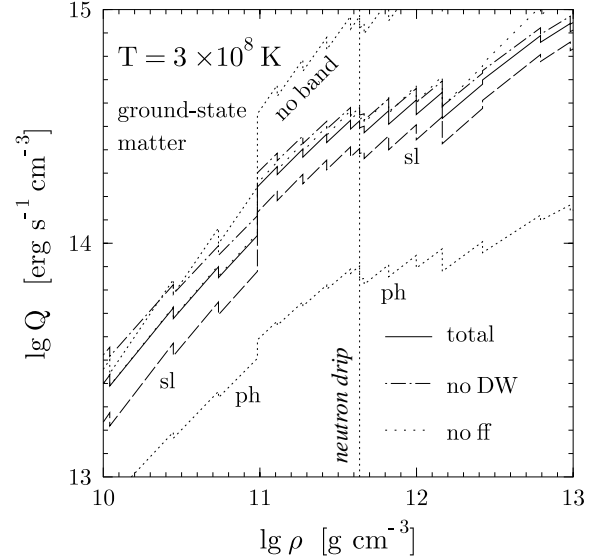

Fig. 8. Density dependence of the neutrino bremsstrahlung emissivity at $T = 3 \times 10^8$ K for ground-state matter calculated with the form factor (11). Solid line: total emissivity. Also shown are: static-lattice contribution (sl), phonon contribution (ph) and the total contributions obtained neglecting either band-structure effects (no band) or Debye–Waller factor (no DW) or nuclear form factor (no ff)

of about 5 at $\rho = 10^{13}$ g cm^{-3}. The effect of the form factor also increases with density while the effect of the Debye–Waller factor becomes lower.

The neutrino emissivities presented in Figs. 3–8 are calculated with the simplified atomic form factor (11) appropriate for a step-like proton distribution within the nuclei. We have verified that the simplified form factor gives quite accurate results for $\rho \lesssim 10^{13}$ g cm^{-3}. However, at higher ρ the neutrino emissivity becomes sensitive to the shape of the proton distribution. Then the form factor based on the proton-density distribution (12) seems to be more reliable, as discussed in Sect. 2. We have made a series of calculations with this more realistic form factor making use of the smooth-composition (SC) model of the ground-state matter (Sect. 2). Fig. 9 is an extension of Fig. 8 to higher densities (10^{12} g cm^{-3} $\leq \rho \leq 8 \times 10^{13}$ g cm^{-3}) for matter containing spherical nuclei. The highest density, $\rho = 8 \times 10^{13}$ g cm^{-3}, is close to the transition to the phases with nonspherical nuclei. We now compare the neutrino emissivities calculated with the realistic and step-like form factors. The realistic form factor is included in both the phonon contribution (through Eq. (21)) and the static-lattice contribution (Sect. 3.3). The emissivities obtained with the realistic form factor for the SC model are compared with those obtained with the step-like form factor for the SC and Negele–Vautherin models of matter. The total emissivities (upper curves) are seen to be close to the static-lattice emissivities (lower curves), which indicates that the static-lattice contribution is dominant. The emissivities in the Negele–Vautherin model show the familiar jumps (e.g., Figs. 7 and 8) associated with variations of the nuclear composition. After averaging over these jumps, they reproduce the emissivities derived in the SC model (with the same form fac-
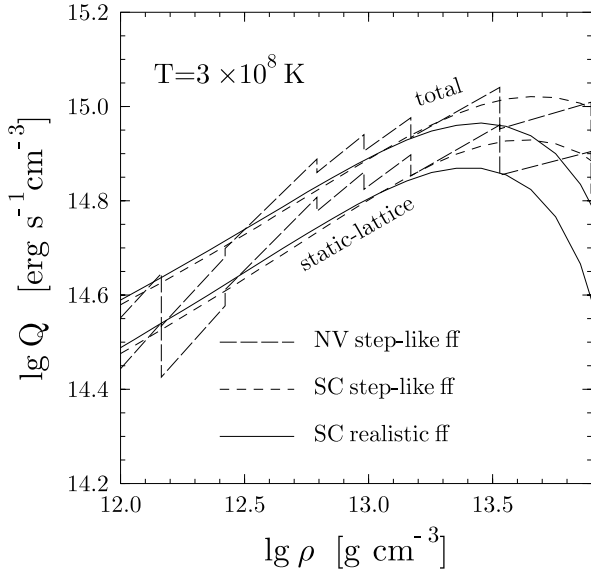
Fig. 9. Density dependence of the bremsstrahlung emissivity at $T = 3 \times 10^8$ K for the ground-state matter composed of spherical nuclei. Long-dashed lines are calculated with the step-like form factor (ff) given by Eq. (11) for the nuclear composition by Negele & Vautherin (NV, 1973). Short-dashed lines are calculated with the same form factor but for the smooth-composition (SC) model of matter (Sect. 2). Solid lines correspond to the SC model and more realistic form factor for the proton distribution (12). Upper lines show the total emissivities, while the lower ones give the static lattice contribution alone

Fig. 10. Density dependence of the bremsstrahlung emissivity at $T = 3 \times 10^8$ K for five phases of spherical and nonspherical atomic nuclei at the bottom of a neutron star crust for the SC model of matter calculated with the realistic form factor. Long-dash line is obtained by assuming the nuclei to be spherical to the crust bottom. Short-dash line is calculated for all phases neglecting the band structure, while dotted line is obtained neglecting the band structure and the form factor

tor). The emissivities obtained with the realistic and step-like form factors are seen to be close for $\rho \lesssim 10^{13}\,\mathrm{g\,cm^{-3}}$. However, when the density becomes higher than $10^{13}\,\mathrm{g\,cm^{-3}}$ the realistic form factor decreases the electron-nucleus interaction and reduces noticeably the neutrino emission compared with the case of the step-like form factor.

Fig. 10 is an extension of Figs. 7–9 towards higher densities. It shows the density dependence of the neutrino bremsstrahlung emissivities through all five phases of spherical and nonspherical nuclei for $T = 3 \times 10^8$ K. In order to display all the phases we use a linear density scale rather than a logarithmic one; ρ_{14} is the density in units of $10^{14}\,\mathrm{g\,cm^{-3}}$. Densities in excess of $1.43 \times 10^{14}\,\mathrm{g\,cm^{-3}}$ correspond to uniform matter in the neutron star core. The emissivities are calculated using the SC model. In the spherical phase, the phonon contribution is included and the Debye–Waller factor is taken into account. In the nonspherical phases, we neglect the Debye–Waller factor and the phonon contribution (see above). This circumstance is partly responsible for the jumps in the neutrino emissivities at $\rho = 9.73 \times 10^{13}\,\mathrm{g\,cm^{-3}}$, the interface between the phases with spherical and cylindrical nuclei. All the curves are calculated with the realistic form factor. The long-dashed curve is obtained assuming the nuclei remain spherical up to the highest densities at the very bottom of the neutron star crust and by including the phonon contribution and the Debye–Waller factor. The parameters of such nuclei are appropriate to the Negele–Vautherin model of dense matter, smoothed over jumps. We also present the emissivities ca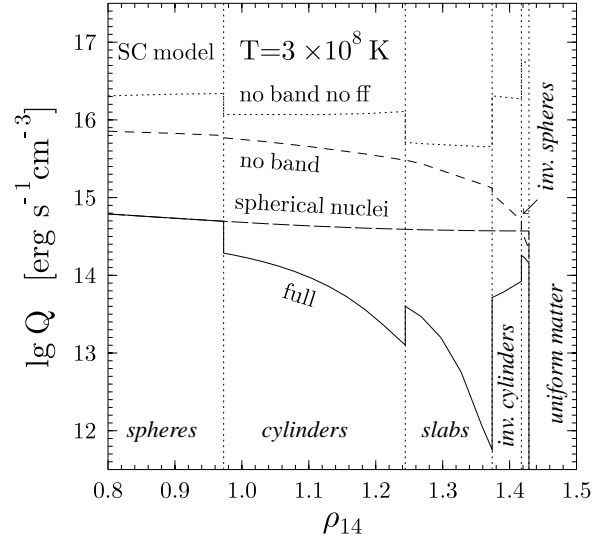lculated for all phases of nonspherical nuclei neglecting either the band-structure effects, or both the band structure and the form factor. The neutrino emission at $\rho \sim 10^{14}\,\mathrm{g\,cm^{-3}}$ is very sensitive to the proton charge distribution. A neglect of the form factor leads to overestimation of the neutrino emissivity by 1–1.5 orders of magnitude. The effects of nonspherical phases are also rather important. Non-sphericity of the nuclei mainly lowers the neutrino emission by reducing the dimension of the sums over reciprocal lattice vectors in Eq. (31). The reduction can exceed one order of magnitude (cf the solid and dashed curves near the cylinder–slab interface). More work is required to calculate the Debye–Waller factor and the phonon contribution and determine accurately the bremsstrahlung emission for nonspherical nuclei. However the spherical–nucleus model probably represents a reasonable upper limit to this emissivity for densities where the nuclei can be nonspherical.

Fig. 11 shows the density dependence of neutrino bremsstrahlung for the ground-state matter of the neutron-star envelopes at six temperatures, from 10^8 K to 1.8×10^9 K, in the density range $10^{10}\,\mathrm{g\,cm^{-3}} \le \rho \le 1.4 \times 10^{14}\,\mathrm{g\,cm^{-3}}$. The $\rho - T$ domain displayed is the most important one for application to neutron-star cooling. The dotted curves are calculated using the Negele–Vautherin model of matter and the step-like form factors (11). The dashed lines are obtained for the SC model with the realistic form factor and on the assumption that nuclei are spherical to the bottom of the crust. The solid lines are also derived for the SC model with the realistic form factor but with allowance for the phases of nonspherical nuclei. Sharp decreases of the curves at $\rho \gtrsim 10^{14}\,\mathrm{g\,cm^{-3}}$ occur because the nuclei become nonspherical (see Fig. 10).
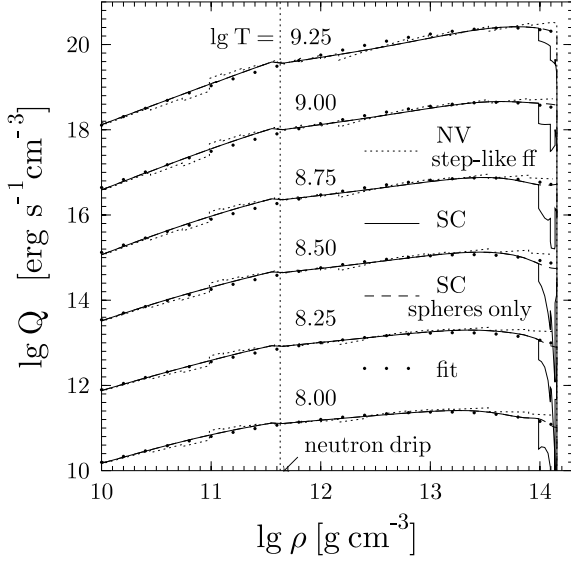
Fig. 11. Density dependence of the bremsstrahlung emissivity for the ground-state matter of the neutron-star crust at six temperatures T in the model by Negele & Vautherin (NV, dots) (1973) with the step-like form factor (ff), and in the SC model with the realistic form factor assuming either the nuclei are spherical to the crust bottom (dashes) or including non-spherical phases (solid lines). Filled circles show our fits (40) to dashed lines

Fig. 12. Density dependence of the neutrino emissivities produced in a neutron star crust and core at $T = 10^9$ K by various neutrino generation mechanisms: electron bremsstrahlung (e-brems), plasmon decay (plasma), Cooper pairing of nucleons (Cooper pairs) in the models of strong (s) and weak (w) neutron superfluidity (SF), and standard neutrino generation mechanisms (N-stand.) in strongly (s) and weakly (w) superfluid uniform matter (see text for details)

Our calculations for spherical nuclei with the realistic form factor in wide density and temperature ranges, $10^9 \, \text{g cm}^{-3} \leq \rho \leq 1.5 \times 10^{14} \, \text{g cm}^{-3}$ and $5 \times 10^7 \, \text{K} \leq T \leq 2 \times 10^9 \, \text{K}$ can be fitted by the expression

$$
\begin{aligned}
\lg Q \, [\text{erg cm}^{-3} \, \text{s}^{-1}] = {} & 11.204 + 7.304\,\tau + 0.2976\,r \\
& - 0.370\,\tau^2 + 0.188\,\tau r - 0.103\,r^2 + 0.0547\,\tau^2 r \\
& - 6.77 \lg(1 + 0.228\rho/\rho_0),
\end{aligned}
\tag{40}
$$

where $\tau = \lg T_8$, $r = \lg \rho_{12}$, and $\rho_0 = 2.8 \times 10^{14} \, \text{g cm}^{-3}$ is the standard nuclear-matter density. The relative error of this fit formula generally does not exceed 1% (in $\lg Q$) over the indicated $\rho - T$ domain. The accuracy of the fit is seen from Fig. 11. The fitting formula reproduces the main features of the neutrino bremsstrahlung radiation in a very wide density domain $10^9 \, \text{g cm}^{-3} \leq \rho \leq 10^{14} \, \text{g cm}^{-3}$, where the atomic nuclei are expected to be spherical, and it probably gives a realistic estimate of the emissivity for higher densities, $10^{14} \, \text{g cm}^{-3} \leq \rho \leq 1.4 \times 10^{14} \, \text{g cm}^{-3}$, where the nuclei become nonspherical. This fit formula should be quite sufficient for many applications.

Finally, in Figs. 12 and 13 we compare neutrino bremsstrahlung by electrons in the neutron-star crust with other neutrino emission mechanisms for $T = 10^9$ K and 10^8 K, respectively. The other mechanisms considered are neutrino emission due to plasmon decay (e.g., Itoh et al. 1996) and due to the nucleon Cooper-pair formation under the action of nucleon superfluidity (e.g., Yakovlev et al. 1998). The SC model of ground-state matter is used. In principle, some contribution at low T may come from neutrino emission due to scattering of electrons by charged impurities (e.g., Haensel et al. 1996). We ignore this
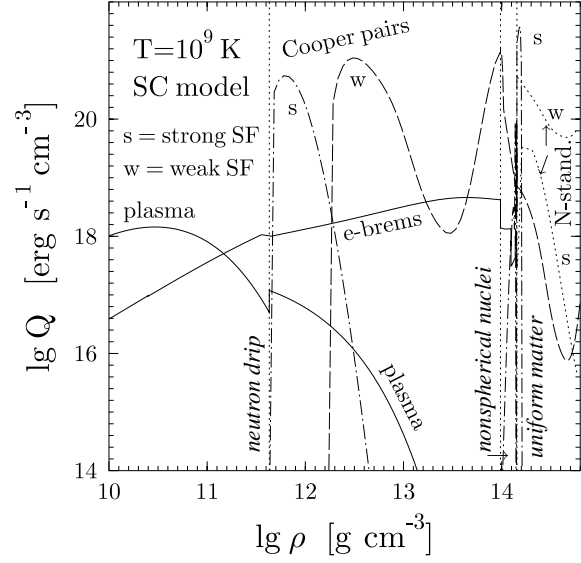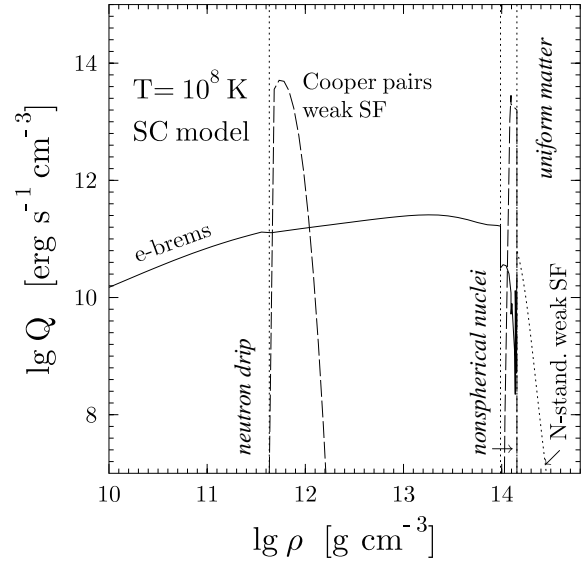

Fig. 13. Same as in Fig. 12 but for $T = 10^8$ K. Plasmon decay, standard neutrino emission from uniform mater and Cooper-pairing emission in the strongly superfluid matter become negligible

mechanism here since it is determined by impurity parameters which are largely unknown. We show also the neutrino emission produced by some mechanisms in uniform matter of the neutron-star core: the standard neutrino energy losses and the nucleon Cooper-pair neutrinos in superfluid uniform matter. It is assumed that uniform matter has a moderately stiff equation of state proposed by Prakash et al. (1988) (the same version as was used by Page & Applegate 1992). The standard neutrino

processes include the modified Urca reactions and nucleon-nucleon bremsstrahlung. All the standard reactions are partially suppressed by the combined action of the neutron and proton superfluids in uniform matter. The reaction rates and suppression factors are taken in the form described by Levenfish & Yakovlev (1996). The proton and neutron superfluid critical temperatures depend on density. We assume singlet-state pairing of protons, and either singlet-state or triplet-state pairing of neutrons. Neutron pairing is expected to occur in a singlet state in matter at densities less than roughly that of the core-crust interface, and in a triplet state at higher densities. For any density we adopt the type of neutron pairing that corresponds to the higher critical temperature. The strong density dependence of the neutrino emissivities in uniform matter (Figs. 12 and 13) is due to the pronounced density dependence of the neutron and proton critical temperatures at $\rho \sim \rho_0$. Since critical temperatures are very sensitive to the microscopic model of the nucleon interaction, we have considered two cases, corresponding to strong (s) and weak (w) nucleon superfluids (SFs). The strong superfluid model is based on the rather large superfluid gaps calculated by Elgarøy et al. (1996) for singlet-state pairing (with maximum gap of about 2.5 MeV as a function of nucleon number density) and by Hoffberg et al. (1970) for triplet-state pairing. The weak superfluid model makes use of the small superfluid gaps derived by Wambach et al. (1993) (with a maximum gap of about 1 MeV) for the singlet superfluid and by Amundsen & Østgaard (1985) for the triplet neutron superfluid. For singlet pairing we regard the weak pairing case to be the more realistic because the calculations of Wambach et al. (1993) included the effects of induced interactions.

The mechanism of neutrino production due to Cooper pairing of nucleons was proposed by Flowers et al. (1976) and independently by Voskresensky & Senatorov (1986, 1987) for uniform matter. A critical comparison of these works has been done by Yakovlev et al. (1998) who considered also the case of triplet neutron pairing. The theory predicts a powerful maximum of the Cooper-pair neutrino emission when the temperature falls below the critical temperature T_c for neutrons or protons. However, at still lower temperatures, $T \ll T_c$, the emission falls exponentially. The emission is much stronger for neutrons than for protons due to the smallness of axial-vector electroweak currents for protons (Yakovlev et al. 1998). In spite of its long history, this process was forgotten for a long time, and it has been included in cooling simulations only recently (Page 1997, 1998; Schaab et al. 1997; Levenfish et al. 1998; Yakovlev et al. 1998). We make use of the results by Yakovlev et al. (1998) for uniform matter and for the crust. In the uniform matter, we take into account neutrino emission due to pairing of neutrons and protons. In the crust, the Cooper neutrino emission is evaluated including the contribution from free nucleons alone (from free neutrons in all phases of matter in the inner crust, and from free protons in the phases with cylinders and spheres of neutrons surrounded by nuclear matter). In principle, there can be a substantial contribution (Yakovlev et al. 1998) from the non-uniform distribution of the nucleons within atomic nuclei

(Sect. 2). We neglect this effect here but we intend to discuss it in a separate article.

In a high temperature plasma, $T = 10^9$ K, at $\rho \lesssim 10^{11}$ g cm^{-3} (Fig. 12), the process most competitive with electron bremsstrahlung is the well-known plasmon decay (Itoh et al. 1996). However its rate falls exponentially with decreasing T, and the process almost dies out at $T = 10^8$ K (Fig. 13). The standard neutrino emission from uniform matter is greatly reduced by the nucleon superfluidity. It decreases exponentially when the temperature becomes much smaller than the superfluid critical temperatures of nucleons. For instance, the standard emission is quite substantial at $T = 10^9$ K but becomes much less significant at $T = 10^8$ K (practically negligible for the case of strong superfluid). Neutrino emission by Cooper pairing in the uniform matter and in the inner crust is also exponentially suppressed when the temperature is much lower than the critical temperatures of neutrons and protons. Accordingly the temperature and density dependence of the Cooper-pair neutrino emissivity is very strong. If $T = 10^9$ K and the superfluidity is strong, we have two peaks of Cooper-pair neutrinos: one near the neutron drip point (at $\rho \sim 10^{12}$ g cm^{-3}), and a very narrow peak near the core-crust interface ($\rho \approx 1.4 \times 10^{14}$ g cm^{-3}). Both peaks are produced by neutron pairing, and are pronounced since the neutron critical temperature is sufficiently small (only slightly exceeds T) in the indicated density ranges even for strong superfluidity. The smallness of T_c in the first density range is associated with a low number density of free neutrons near the neutron drip point, and the smallness in the second density range corresponds to the transition from singlet to triplet neutron pairing. Outside these density ranges the neutron critical temperature is too high and the emissivity of the Cooper neutrinos is exponentially suppressed. When the temperature decreases the emissivity becomes smaller, and the process dies out at $T = 10^8$ K (cf. Figs. 12 and 13).

If $T = 10^9$ K and the superfluidity is weak, the Cooper pairing appears to be the dominant neutrino emission process in a large fraction of the neutron star crust since the neutron critical temperature is not much higher than T. However, the process is practically switched off at low densities $\rho \lesssim 2 \times 10^{12}$ K, because a weak neutron superfluid has not yet occurred at these densities ($T_c < T = 10^9$ K). When the temperature drops to 10^8 K, the neutrino emission due to Cooper pairing is suppressed. Nevertheless, two high peaks of the emissivity survive (similar to those for a strong superfluid at $T = 10^9$ K). The first one corresponds to low $\rho \sim 10^{12}$ g cm^{-3} (T_c is not much higher than 10^8 K), and the second corresponds to $\rho \sim 1.4 \times 10^{14}$ g cm^{-3}, where T_c is low, which corresponds to the transition from a singlet to a triplet neutron superfluid.

We conclude that the main contribution to neutrino emission from a neutron-star crust comes from two processes, the neutrino-pair bremsstrahlung and Cooper pairing of neutrons. The bremsstrahlung neutrino emission has been calculated rather reliably, excluding possibly in the phases of non-spherical nuclei near the core-crust interface. The mechanism operates in a wide ranges of densities and temperatures, and the density dependence of the emissivity is generally smooth. The

neutrino emission due to the Cooper pairing of nucleons is extremely sensitive to the model adopted for the superfluid gaps in the nucleon spectra. This mechanism is more important for lower gaps (weaker superfluid). The emissivity can be a sharp function of density and temperature. We remark that the microscopic models that correspond to weak superfluidity are likely the more reliable since they incorporate the effects of induced processes (screening) in the effective neutron-neutron interaction. In addition, in the phases with non-spherical nuclei, the neutron superfluid gap in the matter is expected to be reduced by the presence of nuclei, in which the matter has a higher density, and a smaller pairing interaction, than in the neutrons outside nuclei. We expect to consider the Cooper-pair process in more detail in a future publication.

5. Conclusions

We have analyzed the neutrino pair emission (1) due to the bremsstrahlung of degenerate relativistic electrons at densities from $10^9 \, \mathrm{g \, cm^{-3}}$ to $1.5 \times 10^{14} \, \mathrm{g \, cm^{-3}}$ and temperatures from 5×10^7 to 5×10^9 K in the neutron-star crusts. We have presented the expressions for the neutrino emissivity from a plasma of liquid and solid atomic nuclei taking into account the effects of finite sizes (the nuclear form factor) of the nuclei. In solid matter, we have studied the static-lattice and phonon contributions to the neutrino bremsstrahlung with allowance for the electron band-structure and multi-phonon processes. We have considered bcc, fcc and hcp Coulomb crystals, and showed that the neutrino emission is insensitive to the lattice type. We have made use of two models of matter in the neutron star crusts: ground-state matter and accreted matter. We have proposed a smooth-composition model of ground-state matter to analyze the neutrino bremsstrahlung near the bottom of the crust, where the shapes of the local nucleon density distributions over Wigner–Seitz cells become important. This smooth-composition model can be applied also for calculating the electron transport properties (thermal and electric conductivities) in the deep layers of the crust. We have calculated the static-lattice contribution for nonspherical nuclei at the very crust bottom, at densities $\rho \gtrsim 10^{14} \, \mathrm{g \, cm^{-3}}$. We have analyzed (Sect. 4) the neutrino emissivity as a function of density, temperature, and nuclear composition. We have obtained a simple analytic fit (40) to the bremsstrahlung emissivity for ground-state matter composed of spherical nuclei in the neutron-star crusts. We expect the fit to give reliable values of the neutrino bremsstrahlung emissivity for densities $\rho \leq 10^{14} \, \mathrm{g \, cm^{-3}}$, where the nuclei are certainly spherical, and to give a reliable upper limit of the emissivity for $10^{14} \, \mathrm{g \, cm^{-3}} \leq \rho \leq 1.4 \times 10^{14} \, \mathrm{g \, cm^{-3}}$, where the nuclei become nonspherical.

Our results can be used, for instance, to study cooling of isolated neutron stars. A not too old star (of age lower than about 10^5–10^6 yr) cools mainly via neutrino emission from its interior (e.g., Pethick 1992). The main contribution to the neutrino luminosity comes usually from the stellar core. However, neutrino emission from the crust can also be important. In young neutron stars it plays a significant role in thermal relaxation of the stellar interiors. It can also be important in rather old neutron stars during the transition from the neutrino cooling stage to the photon one. The neutrino luminosity of the stellar core decays generally somewhat faster than the luminosity of the crust, and the crustal luminosity survives longer. Moreover, the neutrino emission from the crust can dominate the emission from the core in the neutron stars with highly superfluid cores and/or in stars with a stiff equation of state. In the latter case, the crust can be quite massive and its neutrino luminosity can be substantial. Finally, low-mass neutron stars always possess relatively massive crusts, and their neutrino luminosities can be mainly determined by their crusts.

A number of problems remain to be solved in connection with the calculation of neutrino pair bremsstrahlung in the crust. One of these is the influence on the phonon spectrum of neutrons outside nuclei when matter is made up of spherical nuclei. Intuitively one would expect the neutron liquid to make the effective mass of nuclei larger, thereby decreasing phonon frequencies. This in turn would increase the bremsstrahlung from phonon processes at least at low temperatures. Another is the nature of the collective excitations of the phases with non-spherical nuclei. There are a number of these that have low frequencies, and these will give a "phonon contribution", while at the same time affecting the static lattice contribution.

References

Amundsen L., Østgaard E., 1985, Nucl. Phys. 442A, 163

Baiko D.A., Yakovlev D.G., 1995, Astron Lett. 21, 702

Baiko D.A., Yakovlev D.G., 1996, Astron Lett. 22, 708

Baiko D.A., Kaminker A.D., Potekhin A.Y., Yakovlev D.G., 1998, Phys. Rev. Lett. 81, 5556

Brush S.G., Sahlin H.L., Teller E.J., 1966, J. Chem. Phys. 45, 2102

DeWitt H.E., Slattery W.L., Yang J., 1993, In: Van Horn H.M., Ichimaru S. (eds.) Strongly Coupled Plasma Physics. University of Rochester Press, Rochester, p. 425

Dicus D.A., Kolb E.W., Schramm D.N., Tubbs D.L., 1976, ApJ 210, 481

Elgarøy Ø., Engvik L., Hjorth-Jensen M., Osnes E., 1996, Nucl. Phys. A604, 466

Festa G.G., Ruderman M.A., 1969, Phys. Rev. 180, 1227

Flowers E., 1973, ApJ 180, 911

Flowers E., Ruderman M., Sutherland P., 1976, ApJ 205, 541

Haensel P., Pichon B., 1994, A&A 283, 313

Haensel P., Zdunik J.L., 1990, A&A 229, 117

Haensel P., Kaminker A.D., Yakovlev D.G., 1996, A&A 314, 328

Hoffberg M., Glassgold A.E., Richardson R.W., Ruderman M., 1970, Phys. Rev. Lett. 24, 775

Itoh N., Kohyama Y., 1983, ApJ 275, 858

Itoh N., Mitake S., Iyetomi H., Ichimaru S., 1983, ApJ 273, 774

Itoh N., Matsumoto N., Seki M., Kohyama Y., 1984a, ApJ 279, 413

Itoh N., Kohyama Y., Matsumoto N., Seki M., 1984b, ApJ 285, 304

Itoh N., Adachi T., Nakagawa M., Kohyama Y., Munakata H., 1989, ApJ 339, 354; erratum: 1990, ApJ 360, 741

Itoh N., Hayashi H., Nishikawa A., 1996, ApJS 102, 411

Jancovici B., 1962, Nuovo Cim. 25, 428

Levenfish K.P., Yakovlev D.G., 1996, Astron. Lett. 22, 56

Levenfish K.P., Shibanov Yu.A., Yakovlev D.G., 1998, Phys. Scripta (accepted)

Lorenz C.P., Ravenhall D.G., Pethick C.J., 1993, Phys. Rev. Lett. 70, 379

Miralda-Escudé J., Haensel P., Paczyński B., 1990, ApJ 362, 572

Mochkovitch R., Hansen J.P., 1979, Phys. Lett. A73, 35

Nagara H., Nagata Y., Nakamura T., 1987, Phys. Rev. A 36, 1859

Negele J.W., Vautherin D., 1973, Nucl. Phys. A207, 298

Oyamatsu K., 1993, Nucl. Phys. A561, 431

Page D., 1997, ApJ 479, L43

Page D., 1998, Thermal evolution of isolated neutron stars. In: Buccheri R., van Paradijs J., Alpar M.A. (eds.) The Many Faces of Neutron Stars. Kluwer, Dordrecht, p. 539

Page D., Applegate J.H., 1992, ApJ 394, L17

Pethick C.J., 1992, Rev. Mod. Phys. 64, 1133

Pethick C.J., Potekhin A.Y., 1998, Phys. Lett. B427, 7

Pethick C.J., Ravenhall D.G., 1995, Ann. Rev. Nucl. Part. Sci. 45, 429

Pethick C.J., Thorsson V., 1994, Phys. Rev. Lett. 72, 1964

Pethick C.J., Thorsson V., 1997, Phys. Rev. D 56, 7548

Pollock E.L., Hansen J.P., 1973, Phys. Rev. A 8, 3110

Prakash M., Ainsworth T.L., Lattimer J.M., 1988, Phys. Rev. Lett. 61, 2518

Raikh M.E., Yakovlev D.G., 1982, Ap&SS 87, 193

Schaab Ch., Voskresensky D., Sedrakian A.D., Weber F., Weigel M.K., 1997, A&A 321, 591

Soyeur M., Brown G.E., 1979, Nucl. Phys. A324, 464

Voskresensky D., Senatorov A., 1986, Sov. Phys.–JETP 63, 885

Voskresensky D., Senatorov A., 1987, Sov. J. Nucl. Phys. 45, 411

Wambach J., Ainsworth T.L., Pines D., 1993, Nucl. Phys. A555, 128

Yakovlev D.G., Kaminker A.D., 1996, Astron. Lett. 22, 491

Yakovlev D.G., Urpin V.A., 1980, SvA 24, 303

Yakovlev D.G., Kaminker A.D., Levenfish K.P., 1998, Neutrino emission due to Cooper pairing of nucleons in neutron stars. In: Shibazaki N., Kawai N., Shibata S., Kifune T. (eds.) Neutron Stars and Pulsars. Universal Academy Press, Tokyo, p. 195

Young D.A., Corey E.M., DeWitt H.E., 1991, Phys. Rev. A 44, 6508